Eur. Phys. J. D **1**, 57–70 (1998)

THE EUROPEAN PHYSICAL JOURNAL D

Coherent population transfer in NO with pulsed lasers: the consequences of hyperfine structure, Doppler broadening and electromagnetically induced absorption

A. Kuhn[a], S. Steuerwald, and K. Bergmann[b]

Fachbereich Physik der Universität Kaiserslautern, Postfach 3049, 67653 Kaiserslautern, Germany

Received: 11 September 1997 / Revised: 28 October 1997 / Accepted: 29 October 1997

Abstract. Coherent population transfer between vibrational levels of the NO molecule induced by the interaction of two delayed laser pulses, also referred to as stimulated Raman scattering involving adiabatic passage (STIRAP), is studied experimentally in a molecular beam and in the bulk. The consequences of hyperfine splitting and Doppler broadening are discussed in detail. Unlike in previous studies of this kind, transfer occurs simultaneously between more than one group of non degenerate levels. In a molecular beam or in the bulk, the transfer efficiency of STIRAP exceeds that obtained by Stimulated Emission Pumping (SEP) by a factor of 3.6 or 15, respectively. We estimate the absolute transfer efficiency T in the beam to be $T \approx 60\%$, while $T \approx 18\%$ is found in the bulk. In both cases, this is 60% of the maximum value expected from numerical studies. Possible reasons for this discrepancy are discussed. Finally we show that the absorption of a pump pulse in a weakly absorbing medium is significantly enhanced by the presence of a copropagating Stokes pulse when the Rabi frequency Ω_S of the latter is smaller than the width of the Doppler profile $\Delta\nu_D$. The relation of this observation to the phenomenon of Electromagnetically Induced Transparency (EIT), which is observed for $\Omega_S \gg \Delta\nu_D$, is also discussed.

PACS. 33.80.Wz Other multiphoton processes – 33.80.-b Photon interactions with molecules – 42.65.Dr Stimulated Raman scattering; CARS

1 Introduction

Coherent population transfer by a stimulated Raman process involving adiabatic passage (STIRAP) is now an established technique for manipulating the population distribution in atoms and molecules [1]. After the first demonstration with continuous lasers [2] and the subsequent implementation with pulsed lasers [3–5] numerous applications have been proposed or demonstrated. New elements for atom optics [6–8] were developed, applications to atom interferometry [9,10] and laser cooling were reported [11–13] and a concept to use this method to prepare and probe the state of the radiation field in optical cavities has been proposed [14]. The technique was also used to study the collision dynamics of vibrationally excited molecules [15,16]. With some modification the method was furthermore applied for spectroscopic studies [17].

In its simplest form, the STIRAP technique is implemented for a three state system [2,18,19]. Initially state 1 carries the population. The objective is to transfer all the population to a state 3. This is done by suitably timed coupling of an intermediate state 2, typically a state in a different electronic level, to the states 1 and 3 by radiation from a pump laser and a Stokes laser, respectively. Nearly complete population transfer is achieved provided the interaction begins with the Stokes laser and ends with the pump laser. The laser frequencies may be detuned from the resonance with the transition to the intermediate level. However, the two–photon resonance must be maintained. With these conditions met, the system is prepared in a superposition state (called trapped state, discovered in 1976 [20]) with contributions from the bare states 1 and 3, but no contribution from bare state 2. In the adiabatic limit level 2 is not populated in the course of the transfer process and radiative losses from the intermediate state 2 are efficiently suppressed.

The timing of the interactions is done either by pulsing the radiation or, when molecular beams in combination with continuous lasers are used, by spatially shifting the axes of the lasers. In the latter case the particles are exposed to a time dependent radiative coupling as they cross the laser beams. The losses during the transfer process are small, if the evolution is (nearly) adiabatic. Adiabatic evolution depends on several conditions. Firstly, the pulse area of the interaction must be sufficiently large [1,2,21], *i.e.* $\Omega_0 \Delta\tau \gg 1$, where $\Omega_0 = \sqrt{\Omega_{P0}^2 + \Omega_{S0}^2}$ and $\Omega_{P0,\,S0}$ are

[a] current address: Lab. Kastler Brossel, Ecole Normale Supérieure 24 Rue Lhomond, 75231 Paris Cedex 05, France
[b] e-mail: bergmann@rhrk.uni-kl.de

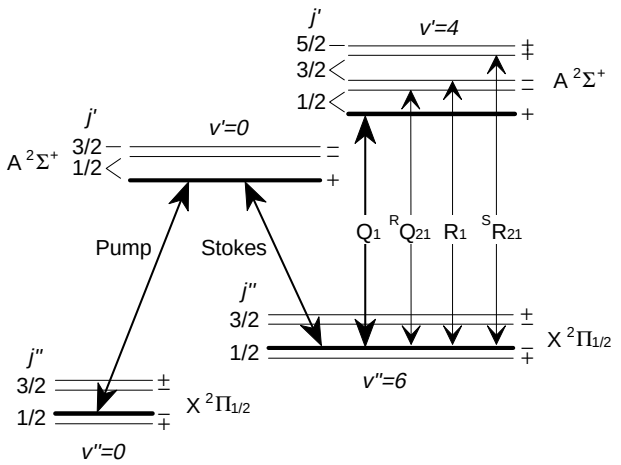

Fig. 1. The level scheme for the NO molecule, relevant for the transfer and the detection.

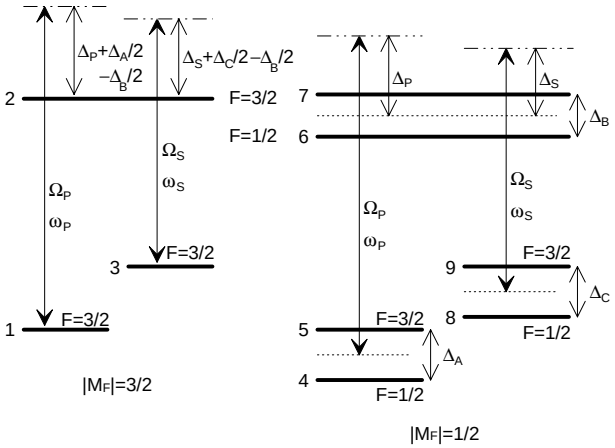

Fig. 2. Details of the level scheme for NO, relevant for the transfer, including the hyperfine structure. Since only the amount of $M_{\rm F}$ is shown, all the levels are doubly degenerate. The levels are numbered from 1 to 9, for convenient reference in the text.

the peak Rabi frequencies of the pulses [22], which measure the coupling strength induced by the lasers; $\Delta\tau$ is the relevant interaction time. Secondly, the frequency fluctuations during the interaction with the atom or molecule with both lasers must be small [3]. Also, deviations from a smooth pulse shape are detrimental. Therefore special care must be taken when implementing the method with pulsed lasers, which usually exhibit inferior coherence properties. In fact, nearly transform limited radiation is required for successful application of the STIRAP technique [4].

Early studies [23] and recent theoretical [24–26] and experimental [27] work has carried the method beyond three level systems. It was found [27] that efficient transfer in multilevel systems can be achieved, subject to some restrictions with regard to the choice of the polarization, frequency and power of the lasers. Also, the consequences of detuning from the two–photon resonance have been analyzed [3,19,28].

In the present work, we expand on previously reported results on coherent population transfer with pulsed lasers applied to the NO molecule [4] as well as on some aspects relevant for population transfer in multilevel systems [27]. We consider in particular the consequences of the hyperfine structure of the molecular levels and the consequences of Doppler broadening.

2 Background

2.1 Some spectroscopic and experimental details

Figure 1 shows the relevant transitions in NO including the level splitting due to Λ-doubling, which is characteristic for molecules in a Π-state. We consider the transfer from the Λ-component with negative parity [29–31] of the lowest rotational state ($j'' = 1/2$) of the vibrational level $v'' = 0$ in the $^2\Pi_{1/2}$ electronic ground state to the ($j'' = 1/2, v'' = 6$) level. The intermediate level is ($j' = 1/2, v' = 0$) in the $A^2\Sigma^+$ electronic state. The wavelength of the pump and Stokes laser is 226 nm and 300 nm, respectively. This coupling leads to the population of only one parity component in the $v'' = 6$ level. The population of this level is monitored by fluorescence induced by excitation to the $v' = 4$ level *via* a Q_1 or $^{\rm S}R_{21}$ transition. Collisional transfer to the adjacent level of different parity is monitored by R_1 or $^{\rm R}Q_{21}$ transitions.

Pulsed radiation with nearly transform limited bandwidth is obtained by pulse amplification of cw radiation [4] with a typical energy of 1 mJ for each of the pulses. The pulse width was $\Delta\tau = 3.0$ ns according to $E(t) = E_0 \exp[-(t/\Delta\tau)^2]$ while the power spectrum had a width (FWHM) of $\Delta\nu_{\rm FL} = 125$ MHz. Very high lying vibrational levels (*e.g.* $v'' \geq 20$) can be populated when coupling occurs to the B–state, which requires radiation with $\lambda < 200$ nm [32]. A spatially smooth intensity profile is needed in the region where the laser and molecular beams cross, in order to assure the validity of the condition for adiabatic evolution near the laser beam axes. Therefore the radiation was spatially filtered, at considerable expense in pulse energy. Typically 0.1 mJ/pulse was delivered to the molecular beam.

2.2 The hyperfine structure

The nuclear spin of $^{14}{\rm N}^{16}{\rm O}$ is $I = 1$ leading to levels with total spin of $F = 1/2$ and $3/2$, see Figure 2. Therefore, what is shown in Figure 1 as a three state system encompasses actually 18 states. Such hyperfine splitting could be detrimental for efficient population transfer since the laser frequencies may not be in two-photon resonance with all radiatively coupled pairs of initial and final levels. However, for linear polarization, when $\hat{E}_{\rm P}$ is parallel to $\hat{E}_{\rm S}$ (this state of polarization was used throughout this experiment), the system decomposes into four independent systems, one each for $m_{\rm F} = \pm 1/2$ and $m_{\rm F} = \pm 3/2$. The latter two are three state systems while the former consist

$$H_6 = -\frac{\hbar}{2}\begin{pmatrix} -2\Delta_P + \Delta_A & 0 & \Omega_{46} & \Omega_{47} & 0 & 0 \\ 0 & -2\Delta_P - \Delta_A & \Omega_{56} & \Omega_{57} & 0 & 0 \\ \Omega_{64} & \Omega_{65} & \Delta_B & 0 & \Omega_{68} & \Omega_{69} \\ \Omega_{74} & \Omega_{75} & 0 & -\Delta_B\Omega_{78} & \Omega_{79} & \\ 0 & 0 & \Omega_{86} & \Omega_{87} & -2\Delta_S + \Delta_C & 0 \\ 0 & 0 & \Omega_{96} & \Omega_{97} & 0 & -2\Delta_S - \Delta_C \end{pmatrix} \tag{2.2}$$

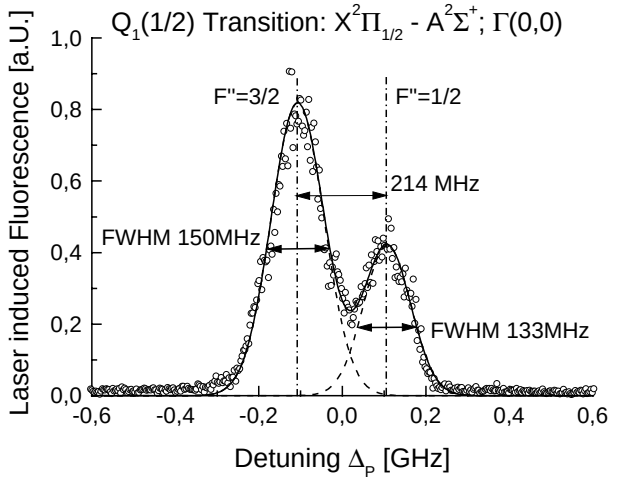

Fig. 3. Laser-induced fluorescence of the $Q_1(1/2)$ level of the X–A -transition. The hyperfine splitting of the ground state is well resolved. The gaussian fit to the profiles reveals a difference in the width of 17 MHz, which is close to the hyperfine splitting of 15 MHz in the upper state. This difference is related to the variation of the linestrength for transitions between (F, m_F)–states, given in Table 1 of the appendix. The ratio of the transition strength $F'' \longrightarrow F' = 1/2$ and $F'' \longrightarrow F' = 3/2$ is 1:8 for $F'' = 1/2$ but 4:5 for $F'' = 3/2$. Therefore, the profile of the peak labeled $F'' = 1/2$ is dominated by the transitions to only one hyperfine component of the upper level, while transitions to both hyperfine levels contribute nearly equally to the peak labeled $F'' = 3/2$, giving rise to a broadening equivalent to the upper state hyperfine splitting.

of six states each. They reduce to effective three level systems since the hyperfine splitting in the electronic ground state is 214 MHz [33] and is spectrally resolved, see Figure 3. The hyperfine splitting in the intermediate state of 15 MHz [34] is small compared to the laser linewidth. The precise value of the difference frequency of the pump and Stokes laser radiation determines between which pairs of levels $(F, |m_F| = 1/2)$ the transfer occurs. Following the numbering shown in Figure 2, transfer may occur between one of the states 4 and 5 to one of the states 9 and 8. When the two-photon resonance is established for the pair of states 4 and 8, the same is true for the pair 5 and 9, since the difference $\Delta_A - \Delta_C$ (see Fig. 3) of the hyperfine splitting in the levels $v'' = 0$ and $v'' = 6$ is negligibly small.

In cases (not encountered here) where the hyperfine splitting in the X-state is not fully resolved additional complications may arise, since transfer from any one of the thermally populated levels 4 and 5 may be transferred to any one of the levels 8 and 9. Such a situation was not encountered in previous studies. In the recent work involving multilevel systems, the initial state was always a single quantum state [27], or the initial level consisted of degenerate quantum states [2].

2.3 The Hamiltonian and dressed state eigenvalues

With reference to the detunings, defined in Figure 2, the Hamiltonian (in rotating wave approximation) [22] for the three-state system, relevant for the $|m_F| = 3/2$ states is

$$H_3 = -\frac{\hbar}{2}\begin{pmatrix} -2\Delta_P - \Delta_A & \Omega_{12} & 0 \\ \Omega_{21} & -\Delta_B & \Omega_{23} \\ 0 & \Omega_{32} & -2\Delta_S - \Delta_C \end{pmatrix}, \tag{2.1}$$

while the six–state Hamiltonian, relevant for the $|m_F| = 1/2$ states reads

see equation (2.2) *above.*

The Rabi frequencies and their dependence on the quantum numbers are explicitly given in Appendix B. It is instructive to inspect the variation of the dressed state eigenvalues for various ratios of the Rabi frequencies and the hyperfine splitting. However, one can not adapt the approach used in [27] because only diabatic crossings arise.

Figure 4 shows the variation of the dressed state eigenvalues for four Rabi frequencies Ω_0 with $\Omega_0/2$ much larger, slightly larger, equal or smaller than the ground state hyperfine splitting. The calculation was done for parallel linear laser polarizations with the laser frequencies tuned to the two-photon resonance for the 4, 8 and 5, 9 pairs of levels. Initially, when only the Stokes laser is present, the system evolves along the horizontal (thick) lines correspond to the trapped states which are, at early times, identical to the initially populated levels 4 and 5. For large Rabi frequencies (Fig. 4a and 4b) a crossing of eigenvalues occurs at early times when the pump laser intensity is zero (or very small). At this time the trapped states have not acquired yet a contribution from the level 8 resp. 9, and the coupling with the states that correlate asymptotically to state 6 resp. 7 is zero. Therefore the crossing is not avoided (or only very weakly avoided) and the system follows the horizontal paths. The dressed states corresponding to these paths correlate to state 8 resp. 9 at late times. The situation is equivalent at the second crossing and thus complete transfer to states 8 and 9 is possible.

For small Rabi frequencies (Fig. 4d), there is no crossing of eigenstates and adiabatic transfer from 4 to 8

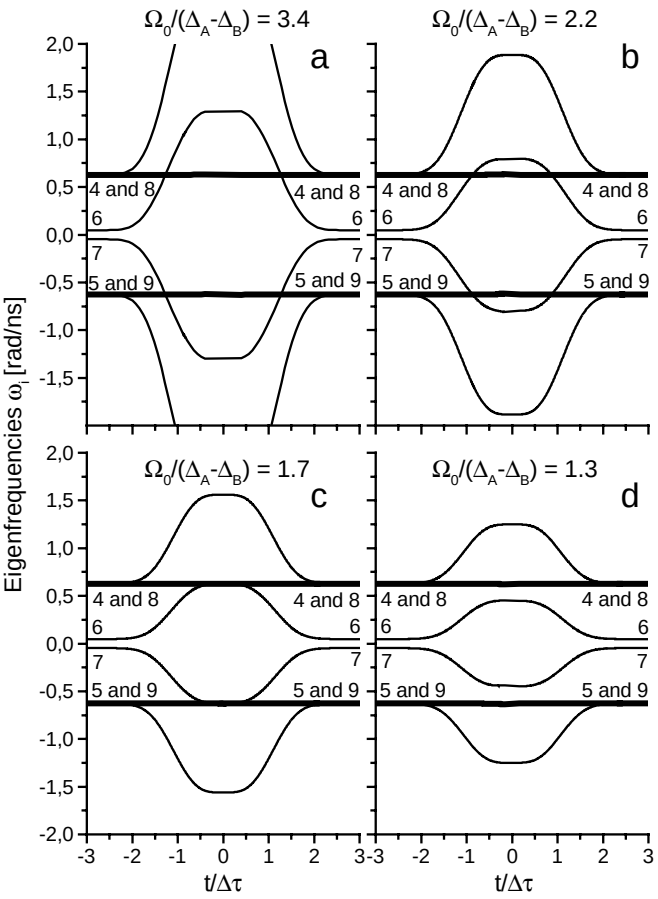

Fig. 4. Evolution of the dressed state eigenvalues of the Hamiltonian (Eq. 2.2), for various ratios of the Rabi frequency and the hyperfine splitting of the ground state level. The horizontal thick line is the adiabatic path for the transfer. The numbers of the bare states (see Fig. 2) which correlate with the eigenvalues at very early and very late times are also given.

(or 5 to 9) is possible, provided the conditions for adiabatic following are met.

Only in the intermediate case (Fig. 4c) where the Rabi frequency matches the hyperfine splitting, the eigenvalues become degenerate near $t = 0$. At this time, the trapped states are superpositions of states 4 and 8 (resp. 5 and 9) and some population will be transferred to the states which asymptotically correlate to 6 resp. 7, from where they will be lost by spontaneous emission.

3 Population transfer in a molecular beam

3.1 Numerical results

Unlike for Na_2 and Ne^* used in previous studies with cw lasers, the electronic lifetime of the NO A–state (200 ns) is long compared to the overall interaction time of 10–20 ns. Therefore, radiative losses from the intermediate state are small during the interaction time with the laser pulses and numerical calculations based on the Schrödinger equation (rather than on the Liouville equation) are adequate. However, any population which reached the intermediate state due to nonadiabatic coupling during the transfer process will later on be lost by spontaneous emission.

The state vector prior to the arrival of the laser pulses is

$$|\Psi(\text{early})\rangle = \frac{1}{\sqrt{3}}(\mathrm{e}^{i\phi_1}|1\rangle + \mathrm{e}^{i\phi_4}|4\rangle + \mathrm{e}^{i\phi_5}|5\rangle). \qquad (3.1)$$

It should be emphasized again, that unlike in our previous studies, more than one non-degenerate quantum state is initially populated. The state vector (3.1) is propagated to

$$|\Psi(\text{late})\rangle = \sum\nolimits_n (c_{n1}\mathrm{e}^{i\phi_1} + c_{n4}\mathrm{e}^{i\phi_4} + c_{n5}\mathrm{e}^{i\phi_5})|n\rangle \qquad (3.2)$$

with $|\Psi(t)\rangle = \hat{T}_t|\Psi(t=0)\rangle$, leading to

$$|\Psi(t)\rangle = \frac{1}{\sqrt{3}}(\mathrm{e}^{i\phi_1}\hat{T}_t|1\rangle + \mathrm{e}^{i\phi_4}\hat{T}_t|4\rangle + \mathrm{e}^{i\phi_5}\hat{T}_t|5\rangle). \qquad (3.3)$$

Levels 1, 4 and 5 are each doubly degenerate. They are thermally populated lacking any fixed relative phases amongst them. Therefore the population in state $|n\rangle$ is given by

$$\langle\Psi(t)|n\rangle\langle n|\Psi(t)\rangle = c^*_{n1}c_{n1} + c^*_{n4}c_{n4} + c^*_{n5}c_{n5} \qquad (3.4)$$

since cross terms vanish.

The transfer efficiency obtained from numerical simulation studies is shown in Figure 5. The panel (a) represents the transfer efficiency as a function of the pump– and Stokes laser detuning on a gray-coded scale. Along the diagonal, the two-photon resonance ($\Delta_\mathrm{P} = \Delta_\mathrm{S}$) is maintained while the frequencies are detuned from the one-photon resonance ($\Delta_0 \neq 0$). The solid line in Figure 5b shows the transfer efficiency "along the diagonal" ($\Delta_\mathrm{P} = \Delta_\mathrm{S}$) as Δ_0 is changed. The dashed line shows the two photon line shape, "perpendicular to the diagonal", *i.e.* for $\Delta_\mathrm{P} = -\Delta_\mathrm{S}$.

The panels (c) and (d) show the related fluorescence intensity. Because the upper state lifetime is long compared to the laser pulse duration, most of the fluorescence is emitted after the population transfer is completed. The pronounced dark resonance, associated with efficient population transfer is obvious from panel (c). Panel (d) shows a horizontal cut (Stokes laser tuned while the pump laser frequency remains on resonance, $\Delta_\mathrm{P} = 0$) through the structure of panel (c). The details of the lineshape depend on the pump laser detuning Δ_P and are similar to the Fano profiles [35] which were also observed by Neusser [17].

The transfer efficiency is slightly reduced for $\Delta_\mathrm{S} = \Delta_\mathrm{P}$, which is even more pronounced when only the transfer from state 4 to state 8, shown in Figure 6, is considered. The loss on resonance is caused by the coupling to states which correlate to level 6 and 7, as discussed in the previous section. Figures 6a and 6b show the transfer from 4 to 8, while the transfer from 4 to 9, which requires tuning of the Stokes laser frequency by 214 MHz, is shown in Figures 6c and 6d. For the latter the relevant Rabi frequencies are smaller (see Appendix), and the condition for adiabatic following is no longer satisfied.

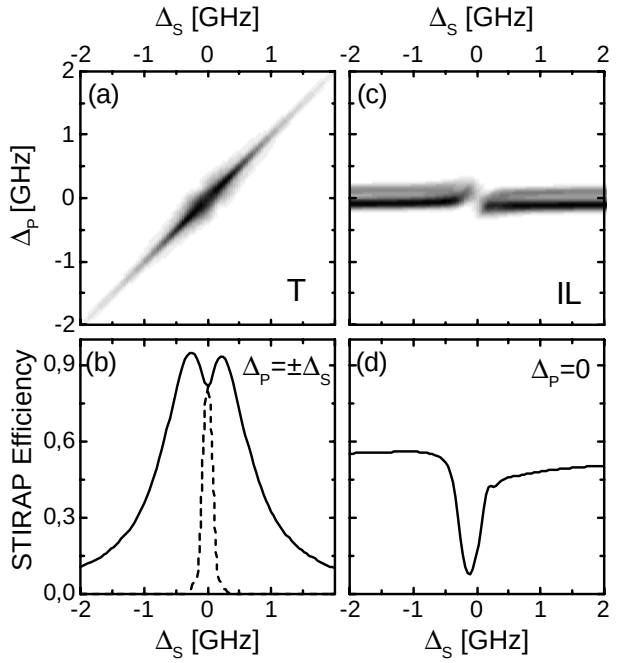

Fig. 5. Numerical simulation of the transfer efficiency (T) shown in (a) and excitation of the intermediate level (IL) shown in (c) as a function of the detunings Δ_P and Δ_S, respectively, in the beam. The solid line (b) shows the transfer efficiency along the contour $\Delta_P = \Delta_S$ (Raman resonance), while the dashed line refers to $\Delta_P = -\Delta_S$. For $\Delta_P = 0$ a pronounced dark resonance is observed (d). The center of the dark resonance is shifted from zero by 107 MHz in the latter panel, because the detunings are measured with reference to the middle between the ground state hyperfine levels (see Fig. 2).

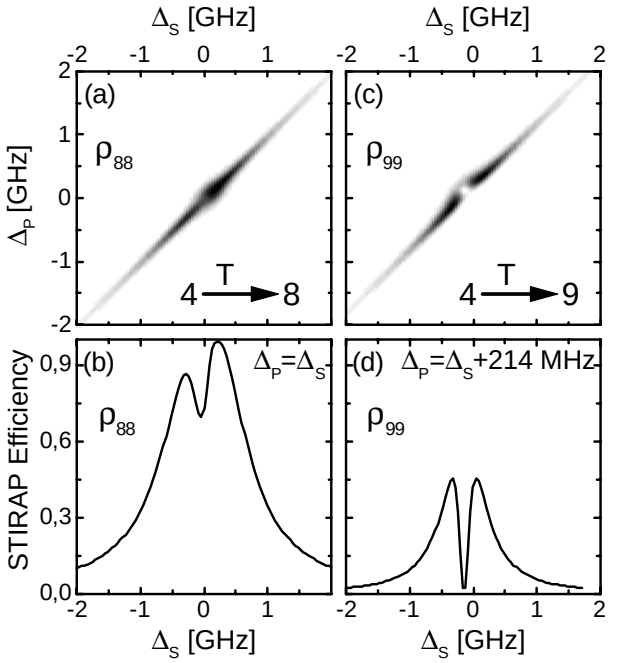

Fig. 6. Numerical Simulation of the transfer in the beam from level 4 to 8 ((a) and (b)) or level 4 to 9 ((c) and (d)) with the frequencies adjusted accordingly (see also the caption of Fig. 5).

3.2 Experimental results

The overall features of the coherent population transfer in NO, observed in the simulation studies discussed in the previous section are well reproduced in the experiment. The population transfer and the related dark resonance is shown in Figure 7 as a function of Stokes and pump laser detuning. The maximum of the Stokes pulse preceded that of the pump pulse by 3 ns. The pump and Stokes laser energies (and beam diameters) were $E_P = 17$ μJ (2 mm) and $E_S = 340$ μJ (4 mm), respectively. The corresponding peak Rabi frequencies for $\Delta m = 0$ transitions from the magnetic sublevels $m = \pm 1/2$ are both $\Omega_0 = 2\pi$ 330 MHz (neglecting the hyperfine splitting, see also appendix A as well as Table 2). With $\Delta\tau = 3$ ns, this leads to $\Omega_0\Delta\tau \approx 6.3$, falling short of the desirable value of $\Omega_0\Delta\tau > 10$.

Figure 7a shows the population in the final state, measured by probe laser induced fluorescence. The signal along the diagonal is related to the STIRAP process. The horizontal structure seen for $\Delta_P = 0$ ($\Delta_S \neq 0$) results from those molecules which are excited to the intermediate level by the pump laser and which decay during the short time interval of 300 ns set for detection about 1 μs after the STIRAP pulse sequence. This fluorescence is a small fraction of the time integrated total fluorescence shown in panel (c), representing the decay from the intermediate level after the excitation to all accessible vibronic levels. Since the simulation studies are based on the Schrödinger equation, the total loss out of the system by spontaneous emission is included, while the population of the initial or final levels by spontaneous emission is not. Therefore the horizontal structure of Figure 7a is not seen in Figures 5a, 6a and 6c.

The transfer efficiency along the ridge of the diagonal structure is displayed in the lower left panel. The maximum transfer efficiency is observed, as expected, very close to the one-photon resonance. The two photon lineshape (recorded for $\Delta_P = -\Delta_S$, *i.e.* along a line which is perpendicular to the "STIRAP-ridge") is also shown.

3.3 STIRAP signature and transfer efficiency

Figure 8 shows the variation of the fluorescence induced by the probe laser as the delay between the pump and Stokes laser is changed from about $\Delta T = -8$ ns (Stokes laser precedes the pump laser) to about $\Delta T = +10$ ns (pump laser precedes the Stokes laser). The maximum of the transfer efficiency near $\Delta T = -3.5$ ns is significantly higher than that for $\Delta T = +2.5$ ns, which is a typical signature of the STIRAP process. For large positive delay, the transfer is caused by Stimulated Emission Pumping (SEP). Obviously, the STIRAP signal exceeds the SEP signal by more than a factor of three.

Experimental determination of the absolute transfer efficiency requires a calibration procedure. When cw lasers

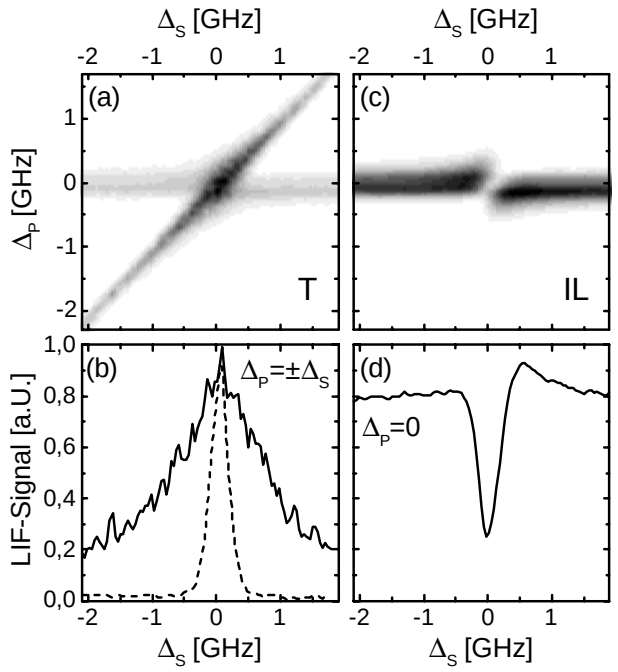

Fig. 7. Experimentally determined transfer efficiency (T) in the beam as a function of the Stokes laser and pump laser detunings shown in (a) and the fluorescence from the intermediate level (IL) shown in (c). Cuts along $\Delta_P = \Delta_S$ ((b), solid line, Raman resonance), $\Delta_P = -\Delta_S$ ((b), dashed line), or for $\Delta_P = 0$ ((d), exhibiting the dark resonance) are also shown. The horizontal structure seen in (a) shows that the spontaneous emission of the population from the intermediate level still contributes to the fluorescence signal. Most of these molecules do not reach the final level and therefore this process is not included in the numerical studies (Fig. 5).

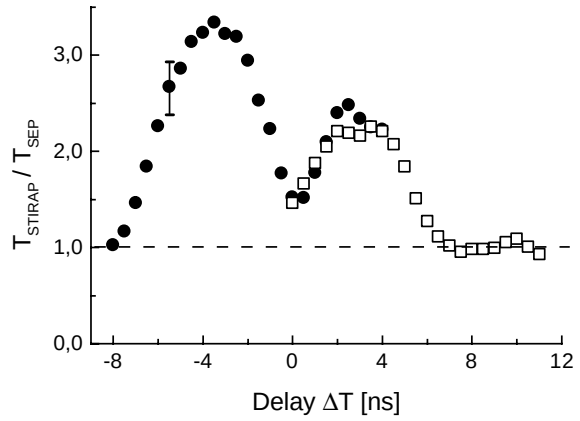

Fig. 8. Experimentally determined ratio $T_{\mathrm{STIRAP}}/T_{\mathrm{SEP}}$ of the population transfer efficiency T *in the beam* as a function of the delay between the pulses (STIRAP-signature). Negative delay corresponds to the STIRAP configuration (Stokes pulse precedes the pump pulse) while positive delay relates to the SEP configuration (pump pulse precedes Stokes pulse). The results from two different runs are combined. The transfer observed at large positive delay is used to calibrate the absolute transfer efficiency.

are used for the transfer *via* an electronic state, the radiative lifetime of which is short compared to the interaction time with the laser, the normalization procedure is straightforward and unambiguous [2,27]. Under those circumstances the pump laser alone will deplete all the population of the initial state by optical pumping. The fraction of the population, which reaches the final state by spontaneous emission is determined from the known transition strength. Thus, the ratio of the laser-induced fluorescence out of the final state for the STIRAP transfer to the fluorescence when only the pump laser is present provides an accurate measure of the transfer efficiency.

The attempt to use the pump laser induced spontaneous emission to the final state for calibration fails here, because pump laser induced Rabi oscillations occur which are not damped during the interaction time. Therefore the fraction of molecules residing in the electronic state after the pump laser pulse is over depends sensitively on the pulse area $\Omega_{\mathrm{P0}}\Delta\tau$. In fact, it may range between zero and 100%. However if $\Omega_{\mathrm{P0}}\Delta\tau \gg 1$, and pulse-to-pulse fluctuations are large enough, on the average 50% of the molecules will be in the excited state at the end of the pump pulse. Thus 50% of the molecules (rather than 100%) will radiatively decay, the fraction of molecules reaching the final state is again known and can be used for the calibration, as demonstrated in the recent work on SO_2 [5]. Here, we adopt a different approach. When the pump laser precedes the Stokes laser with no overlap between the two but the delay ΔT is still small compared to the radiative lifetime, molecules are first excited to the intermediate state by the pump laser and then transferred to the final state by stimulated emission pumping. If the pulse areas of both lasers are large enough and the signal is accumulated for a sufficiently large number of pulses, the pulse-to-pulse fluctuations will average over the Rabi oscillations and a known fraction of the molecules will be found in the final state.

For this experiment the collimation of the molecular beam is such that the residual Doppler width related to the motion perpendicular to the molecular beam axis is small compared to the laser linewidth. Therefore the detuning of the laser frequencies from their respective transition frequencies is the same for all the molecules in the beam and the consequences of the hyperfine splitting for the normalization procedure need to be carefully considered. In the Stimulated Emission Pumping (SEP) configuration ($\Delta T > 6$ ns, see Fig. 8), the molecules are excited to the intermediate level by a pump laser induced one-photon process, in which the hyperfine structure of the initial state is resolved, *i.e.* only the population of one hyperfine component is transferred to the intermediate state. Here we tune the pump laser frequency to the $F'' = 3/2$ level which carries 2/3 of the total population accessible for coherent population transfer. The fraction of 25% of that population, *i.e.* 16.7% of the total population of the initial $j'' = 1/2$ level, will be transferred to the final level in the SEP process. The STIRAP process will transfer the population of both levels $F'' = 1/2$ and 3/2 since the Raman resonance for transitions out of these levels is the

same. Since the STIRAP signal exceeds that one obtained with SEP by a factor of 3.6, the transfer efficiency of the STIRAP process is 60%.

There are several possible causes which may have prevented us from reaching a transfer efficiency closer to unity than actually observed. We first mention two aspects which, at first glance, seem to contribute to the difficulties. Closer inspection shows, that they can't be the major cause of the problem:

- the line strength factors, see Table 3, vary by nearly one order of magnitude with m_F and at first glance it may seem that the mean Rabi frequency overestimates the value of $\Omega\Delta\tau$ for transfer out of same levels and thus non adiabatic coupling may have been stronger than expected. However, when the line strength factors are summed over the $F' = 1/2$ and $F' = 3/2$ levels in the upper state, which are not resolved, the effective linestrength factors are independent of m_F;
- the bandwidth of the laser were larger than measured when the data in the SEP regime was taken, transfer out of the $F = 1/2$ level would have been possible. The higher transfer efficiency in the SEP regime would increase the transfer efficiency in the STIRAP regime accordingly. We emphasize, however, that saturation broadening does not occur for excitation with coherent pulses, *i.e.* for radiation with transform limited bandwidth (see Append. C).

The lower than expected transfer efficiency could have been caused by the following:

- despite spatial filtering, the profile of the laser beams may have been less uniform than anticipated. This would locally lead to an effective Rabi frequency smaller than estimated;
- depending on the alignment of the Nd:YAG laser, the pump pulse could have been of asymmetric shape. If, for instance, the fall time is longer than the rise time, the ratio Ω_S/Ω_P would not approach zero as needed. Therefore, some of the population in the dark state would coherently return to the initial levels. On the other hand, for large negative delay (Stokes precedes pump, with no overlap expected), an asymmetric pulse shape would lead to a transfer signal which is larger than expected from pump laser induced fluorescence (Franck-Condon pumping). Such enhanced transfer is indeed observed for $\Delta T = -8$ ns, see Figure 8.

4 Population transfer in Doppler broadened media

Here we consider the feasibility of efficient population transfer in the bulk. We show that Doppler broadening is detrimental to the success of STIRAP when exciting high lying vibrational states of the NO molecule, but that it might be applied successfully in other cases with a small energy difference between initial and final levels.

We examined NO at a pressure of $p = 0.1$ mbar and at room temperature. For $T = 300$ K, we have $kT/\omega_c \approx 0.1$

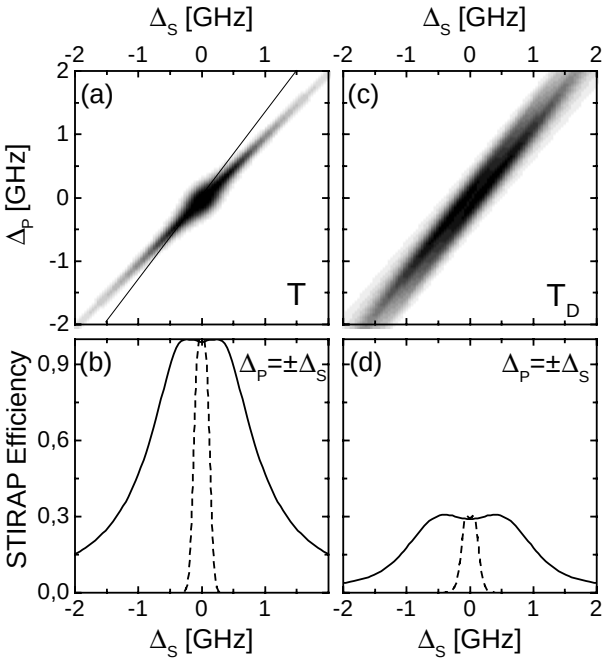

Fig. 9. Comparison of the results of numerical simulation studies of the transfer efficiency in the beam (T, shown in (a) and (b)) and in the bulk (T_D shown in (c) and (d)) for $\Omega_0\Delta\tau = 9$ and $\Delta\tau = 3$ ns. The cuts along the Raman resonance ($\Delta_P = \Delta_S$, solid lines, see also thin line in (a)) and perpendicular to it ($\Delta_P = -\Delta_S$, dashed lines) are also shown.

and only the vibrational state $v'' = 0$ of the electronic ground state $X^2\Pi$ carries significant population. There is, however, a broad rotational distribution with its maximum at $j'' = 10.5$. In the experiments we use $j'' = 5.5$.

4.1 Numerical results

The transfer efficiency $T_0(\Omega_P, \Omega_S, \Delta_P, \Delta_S)$ depends on the Rabi frequencies and the detunings. In a Doppler broadened medium, the effective detuning depends on the velocity component along the direction of the laser beam

$$\Delta_P^{\text{eff}} = \Delta_P + v/\lambda_P \qquad \Delta_S^{\text{eff}} = \Delta_S + v/\lambda_S. \tag{4.1}$$

The overall transfer efficiency

$$T_D(\Delta_P, \Delta_S) = \int f(v) T_0(\Delta_P + v/\lambda_P, \Delta_S + v/\lambda_S)\mathrm{d}v \tag{4.2}$$

is obtained by integration over the velocity distribution

$$f(v)\mathrm{d}v = \frac{1}{\bar{v}_x\sqrt{\pi}}\,\mathrm{e}^{-(v/\bar{v}_x)^2}\,\mathrm{d}v. \tag{4.3}$$

Results are shown in Figure 9 for $\bar{v}_x = 408$ m/s, $\lambda_P = 226$ nm and $\lambda_S = 300$ nm, in comparison with those for a collimated molecular beam ($\bar{v}_x = 0$). Obviously, the Doppler broadening reduces the overall transfer efficiency

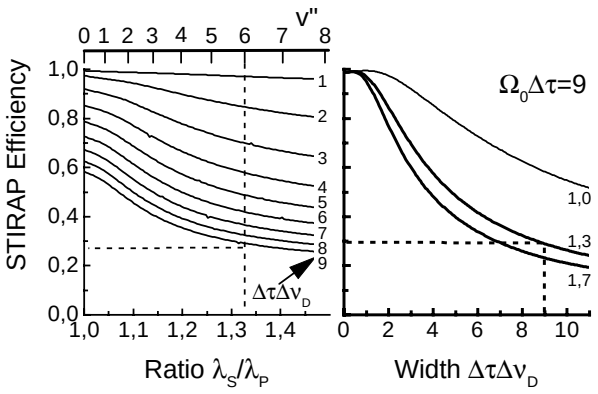

Fig. 10. Simulation of the STIRAP transfer efficiency in Doppler broadened media as a function of the ratio λ_S/λ_P and the product $\Delta\tau\Delta\nu_{\rm Doppler}$. The relevant λ_S/λ_P ratios for the population of specific vibrational levels v'' in the NO molecule are indicated. Here we have $\lambda_P = 226$ nm and $v'' = 6$ is excited with $\Delta\tau\Delta\nu_{\rm Doppler} = 9$, therefore a transfer efficiency of 29% is expected.

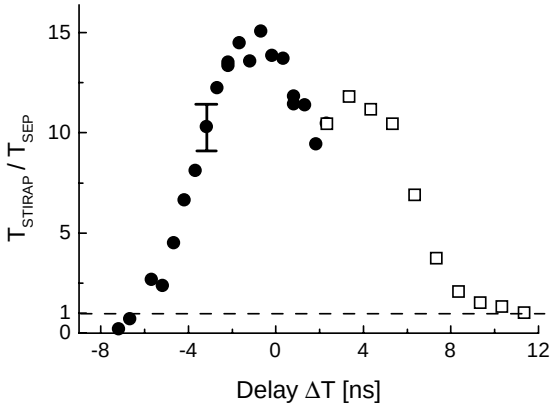

Fig. 11. Experimentally determined ratio $T_{\rm STIRAP}/T_{\rm SEP}$ of the population transfer efficiency T *in the bulk* as a function of the delay between the pulses (STIRAP-signature). Negative delay corresponds to the STIRAP configuration (Stokes pulse precedes the pump pulse) while positive delay relates to the SEP configuration (pump pulse precedes Stokes pulse). The results from two different runs are combined. The transfer observed at large positive delay is used to calibrate the absolute transfer efficiency.

to less than 1/3 as compared to the beam results. It is, however, significantly higher than for SEP, see below.

For $\lambda_P = \lambda_S$, the two photon resonance is maintained independent of the detuning due to the Doppler shift. The integration (Eq. (4.2)) is then along the two photon resonance line (the diagonal in Fig. 9). With increasing velocity, the frequencies are detuned further from the resonance with the intermediate level and a higher Rabi frequency is needed to guarantee adiabatic following.

For $\lambda_P \neq \lambda_S$, the Doppler broadening is significantly more detrimental, since the Doppler shift of the pump and Stokes laser is only partially compensated. With increasing velocity, the system will tune off the two photon resonance, and adiabatic following is no longer possible. The integration (Eq. (4.2)) is along a path which is tilted with respect to the diagonal, see Figure 9.

The dependence of the efficiency $T_D(\Delta_P = \Delta_S = 0)$ on the ratio λ_S/λ_P and the product $\Delta\tau\Delta\nu_{\rm Doppler}$, where $\Delta\nu_{\rm Doppler}$ is the Doppler width, is depicted in Figure 10. Almost complete inversion of a three level system can be achieved for $\lambda_S/\lambda_P \longrightarrow 1$ and/or for higher peak Rabi frequencies (not available for this experiment).

The STIRAP efficiency for excitation of $v'' = 6$ would increase to 85% when the product $\Delta\tau\Delta\nu_{\rm Doppler}$ is reduced by a factor 5. This could be achieved either by cooling or by using shorter pulses. If the pulse length decreases the pulse energy must increase in order to maintain the pulse area.

4.2 Experimental results

The transfer efficiency T_D from $(v'' = 0, j'' = 5.5)$ to $(v'' = 6, j'' = 5.5)$ *via* $v' = 0$ in the A-state in the bulk is shown in Figure 11 as the time delay of the pulses is changed. The STIRAP signature is again clearly seen.

From the laser pulse energies ($E_P = 60$ μJ, $E_S = 300$ μJ) and the beam diameters ($D_P = D_S = 3$ mm), we estimate the Rabi frequencies to be $\Omega_{P0} = \Omega_{S0} = 2\pi$ 480 MHz, averaged over the magnetic sublevels of NO.

Figure 11 shows a dramatic enhancement of the transfer efficiency in the STIRAP regime as compared to the SEP regime. This enhancement is significantly larger in the bulk than in the beam. In the bulk, only a small fraction of the molecules, essentially given by the ratio of the laser linewidth over the Doppler linewidth ($\approx 4.7\%$), participates in the SEP process (concerning the absence of power broadening in this experiment, see append. C). Since partial Doppler compensation occurs in the STIRAP process, a larger fraction of the molecules is addressed in this case.

Detection of the molecules in $v'' = 6$ is done by laser induced fluorescence. The bandwidth of the excimer laser pumped dye laser used in this case was large compared to the Doppler width. Therefore the detection efficiency is independent of the velocity of the molecules. The hyperfine splitting is more than one order of magnitude smaller than the Doppler width and can be neglected here. Therefore the SEP process reaches an efficiency of

$$E_{\rm SEP} \approx 0.25 \times 4.7\% = 1.2\%. \qquad (4.4)$$

The transfer efficiency of the STIRAP process is 15 times larger than for SEP, *i.e.* $E_{\rm STIRAP} = 18\%$. As in the beam experiments, this is only 60% of the value expected from the calculation.

5 Stokes laser induced absorption in a Doppler broadened medium

Pulse propagation effects in absorbing media have recently attracted much interest [36–39]. Harris and coworkers [40] as well as others (see *e.g.* [41]) demonstrated the phenomenon of Electromagnetically Induced Transparency

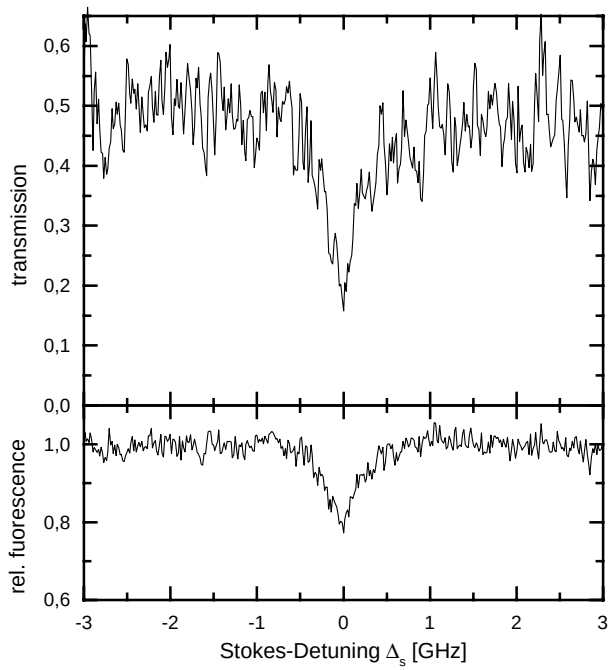

Fig. 12. Transmission of the pump pulse embedded in the Stokes pulse (*i.e.* zero delay), upper panel, and laser induced fluorescence from the intermediate level, lower panel, as a function of the Stokes laser detuning Δ_S. The pump laser was tuned to resonance $\Delta_P = 0$ while the Rabi frequencies were $\Omega_{P0} \approx 2\pi$ 140 MHz and $\Omega_{S0} \approx 2\pi$ 370 MHz.

(EIT) in lead vapor. In their experiment, strongly absorbing lead vapor was made transparent for pump laser radiation when its pulse envelope was embedded in the envelope of a powerful Stokes pulse. The Rabi frequency of the latter was $\Omega_S > 2\pi$ 160 GHz and thus much larger than the Doppler width. Therefore a Doppler shift has only a negligible effect. Here we show that a related mechanism, which leads to EIT when $\Omega_S \gg \Delta\nu_D$, results in Electromagnetically Induced Absorption (EIA) when we have $\Omega_S \leq \Delta\nu_D$. The connection of EIT and STIRAP is discussed in some more detail in [42]

5.1 Experimental results

In the experiment, we observe the transmission of a pump laser pulse ($\Omega_P = 2\pi$ 140 MHz) after propagation through a 300 mm long cell containing NO at $T = 300$ K. A pressure of 0.4 mbar was chosen to adjust the absorption of the pump pulse resonant with the $Q_1(5.5)$ line of the $\gamma(0,0)$ band to 50%.

We compare the absorption of the pump laser pulse ($\Delta\tau_P = 2.7$ ns) with and without copropagating Stokes laser pulse ($\Delta\tau_S = 3.1$ ns, $\Omega_S = 2\pi$ 370 MHz, no time delay). Figure 12 shows the transmission of the pump laser as the Stokes laser frequency is tuned. On two photon resonance, the transmission drops from 50% to about 15%. This confirms that the pump laser pulse is indeed more strongly absorbed when embedded in a copropagating resonant Stokes laser pulse. In parallel, we also observe a

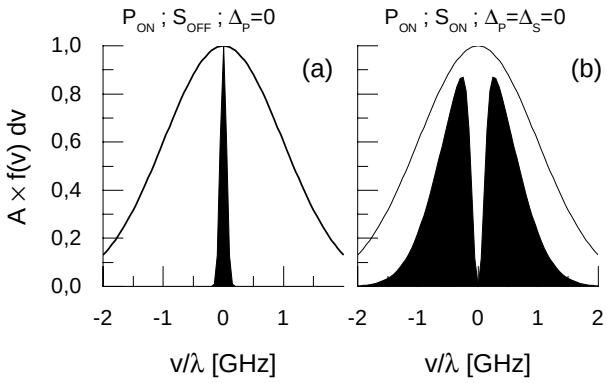

Fig. 13. Velocity distribution of the molecules in the cell (solid lines). The fraction of molecules contributing to absorption is shaded, with the pump laser alone (tuned to resonance) and the pump laser together with the Stokes laser (tuned to the Raman resonance) are shown on the left and right side, respectively. With the Stokes laser present, molecules with $v \approx 0$ do not absorb the pump laser radiation anymore (EIT). However, otherwise inactive molecules in a large range of velocities $|v| > 0$ may contribute (EIA). The net result is a significantly enhanced absorption.

significant reduction of the fluorescence from the intermediate level about half way along the absorption path. This signifies that the absorption due to resonant one photon excitations of the intermediate level is reduced, whereas the enhanced overall absorption must be a result of two photon processes, *i.e.* Raman excitations to $v'' = 6$.

5.2 Induced transparency *vs.* absorption

Figure 13a shows the range of velocity which leads to a Dopplershift of no more than the laser bandwidth. These molecules (a fraction of about 5%) contribute to the absorption. With the Stokes laser present and tuned to resonance, pump laser radiation can not be absorbed by molecules with $v \approx 0$. This group of molecules experiences electromagnetically induced transparency, like in the experiments by Harris. In those experiments, the range over which absorption is eliminated is of the order of 150 GHz and thus covers all of the Doppler width. In our experiments, however, the Rabi frequency is of the order of the Doppler width and molecules in a large range of velocities are tuned, because of their Doppler shifted frequencies, into resonance with the components of the Stark doublet (the fraction of molecules is shown in Fig. 13b). The net effect is a strongly enhanced absorption.

In order to observe the EIA process discussed here, one typically needs a medium with an initial transmission of about 50% which can be reduced to a much smaller value when the Stokes laser pulse is copropagating.

It is interesting to see, that it is the magnitude of $\Omega_S/\Delta\nu_D$ which controls the consequences of the presence of the Stokes laser; EIT is observed for $\Omega_S/\Delta\nu_D \gg 1$, while $\Omega_S/\Delta\nu_D \leq 1$ leads to EIA. Obviously, there is a value of $\Omega_S/\Delta\nu_D$ for which the Stokes laser has no effect on the transmission of the pump laser.

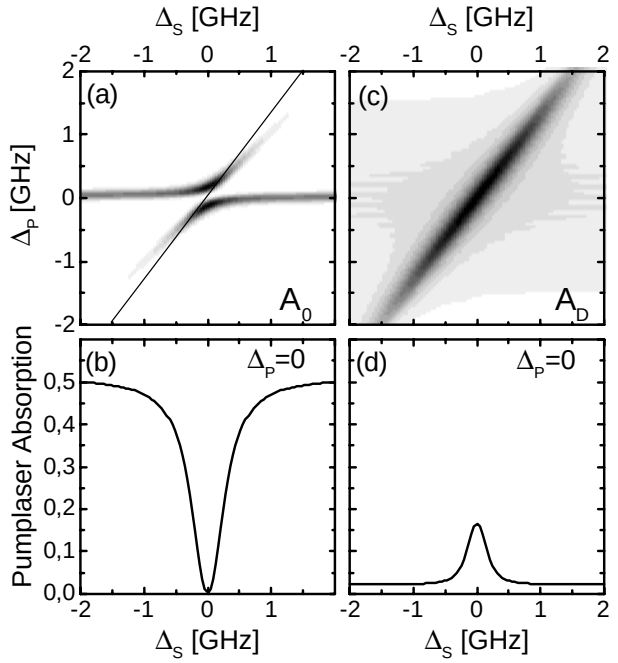

Fig. 14. Comparison of the pump laser absorption under the influence of the Stokes laser in the beam (A_0 shown in (a)) and in the bulk (A_D shown in (c)). The lower panels show the absorption for $\Delta_P = 0$ as a function of Δ_S. In the beam ((b), no Doppler broadening), the absorption vanishes at the Raman resonance. In the bulk ((d), Doppler broadening), the absorption reaches a maximum when $\Delta_P = \Delta_S = 0$. The integration path used to determine $A_D(\Delta_P = \Delta_S = 0)$ is indicated in (a).

In Figure 14, the pump laser absorption without Doppler broadening (left hand side) is compared to the absorption of a Doppler broadened medium (right hand side) as a function of pump- and Stokes laser detuning. The parameters for the numerical simulation correspond to the experimental conditions (see section 5.1). It is seen that the absorption drops to zero without Doppler broadening but raises up to 16% in the Doppler broadened medium. Due to the dynamic Stark shift, the peaks of the absorbing Stark doublet are shifted towards the Raman resonance line $\Delta_P = \Delta_S$. The path of the Doppler integral, indicated in Figure 14a, runs almost parallel to this line, thus increasing the number of molecules participating to the absorption process. The ratio λ_S/λ_P determines the direction of the integration path and controls the relative contribution of EIT and EIA. For the parameters used here, the medium becomes transparent for $\lambda_S/\lambda_P \leq 0.7$.

6 Summary and conclusion

We have expanded our previous studies of coherent population transfer to a vibrationally excited level of the NO molecule. In particular we have analyzed the consequences of hyperfine splitting and Doppler broadening for the transfer efficiency.

In previous STIRAP studies, the initial level consisted of a single quantum state or of a group of degenerate sublevels. Here we transfer simultaneously population from two groups of non-degenerate levels to two such groups in the vibrationally excited state. Since the hyperfine splitting is larger than the bandwidth of the laser and both radiation fields are linearly polarized parallel to each other, complications, such as demonstrated and analyzed by Martin *et al.* [27], do not occur. We have also discussed, in some detail, the normalization procedure needed to determine the absolute transfer efficiency. A discrepancy between the expected and observed efficiencies is found, the reason for which has not yet been identified unambiguously.

We have also studied population transfer in the bulk with a Rabi frequency Ω_0 smaller than the Doppler width $\Delta\nu_D$. The STIRAP transfer efficiency is more than an order of magnitude larger than that obtained by Stimulated Emission Pumping (SEP), since a partial compensation of the Doppler shift occurs in the coherent two photon process, allowing a larger fraction of molecules to participate in the transfer.

Finally we considered the effect of a Stokes laser pulse copropagating with a pump laser pulse in a weakly absorbing medium. While the phenomena of Electromagnetically Induced Transparency (EIT) is observed when $\Omega_S \gg \Delta\nu_D$, we observe an enhanced absorption (EIA), since $\Omega_S \leq \Delta\nu_D$, since the number of molecules which are able to absorb a photon increases due to the Stark shift and splitting at resonance. Thus, the EIT or the EIA phenomena could be used to open or close, respectively, a light path in a laser controlled optical gate.

Financial support by the Deutsche Forschungsgemeinschaft and partial support by the EU (HCM network ERB-CHRXCT-94-0603) is acknowledged. A.K. is indebted to the Alexander von Humboldt-Stiftung for support.

Appendix A: Rabi frequencies

The population of a two level system exposed to coherent, resonant radiation oscillates between the levels with the Rabi frequency $\Omega = \boldsymbol{\mu} \cdot \boldsymbol{E}/\hbar$, where E is the amplitude of the radiation field. Evaluation of the dipole matrix element μ is a non trivial task because of the large manifold of rotational sublevels and the mixtures of Hunds cases a and b in the $X^2\Pi$ state of NO. Therefore, we compile the necessary information in this appendix.

A.1 Dipole moments of NO

The coupling schemes in the A and X states of NO are different. This leads to different sets of quantum numbers, (v', j', m', k') and (v'', j'', m'', Ω) respectively, which specify the rovibronic substates. The parity splitting in the X state and the hyperfine splitting are not considered in equations (A.1 and A.2). The squared dipole moment of

Table 1. Hönl-London factors and dipole matrix elements for the various pump and Stokes transitions of the NO $\gamma(0,0)$ and $\gamma(0,6)$ bands, assuming linear polarization ($\Delta m = 0$) for $j'' = 1/2$ and $j'' = 3/2$.

				$\mu_{0,0}[10^{-31}$ Asm]		$\mu_{0,6}[10^{-31}$ Asm]		
j''	Transition	Line	HLF	$\pm 1/2$	$\pm 3/2$	$\pm 1/2$	$\pm 3/2$	$\leftarrow m''$
1/2	$^2\Sigma^+$	Q_1	0.667	2.135	–	0.968	–	
		Q_{21}	0.667	2.135	–	0.968	–	
	$\updownarrow$	R_1	0.333	1.510	–	0.684	–	
	$^2\Pi_{1/2}$	R_{21}	0.333	1.510	–	0.684	–	
3/2	$^2\Sigma^+$	P_1	0.362	1.573	–	0.713	–	
		P_{21}	0.306	1.447	–	0.656	–	
	$\updownarrow$	Q_1	1.112	0.872	2.616	0.395	1.186	
	$^2\Pi_{1/2}$	Q_{21}	1.022	0.836	2.508	0.379	1.137	
		R_1	0.616	1.590	1.298	0.721	0.588	
		R_{21}	0.582	1.545	1.262	0.701	0.572	
	$^2\Sigma^+$	P_{12}	0.972	2.578	–	1.169	–	
		P_2	1.028	2.652	–	1.202	–	
	$\updownarrow$	Q_{12}	0.756	0.719	2.157	0.326	0.978	
	$^2\Pi_{3/2}$	Q_2	0.846	0.761	2.282	0.345	1.034	
		R_{12}	0.184	0.869	0.709	0.394	0.322	
		R_2	0.218	0.946	0.772	0.429	0.350	

a specific A $\longrightarrow$ X transition reads [43]

$$\begin{aligned}\mu^2 &= |\langle \mathrm{A}, v', j', m', k'|d_q|\mathrm{X}, v'', j'', m'', \Omega\rangle|^2 \\ &= \mu_{\mathrm{el}}^2\ \mathrm{FCF}_{v'v''}\ |\langle j', m', k'|d_q|j'', m'', \Omega\rangle|^2 \\ &= \mu_{\mathrm{el}}^2\ \mathrm{FCF}_{v'v''} \begin{pmatrix} j' & 1 & j'' \\ m' & -\Delta m & m'' \end{pmatrix}^2 |\langle j', k'|d_q|j'', \Omega\rangle|^2,\end{aligned} \tag{A.1}$$

where d_q is the dipole operator ($q = 0$ for excitation with linearly polarized light) and $|\langle j', k'|d_q|j'', \Omega\rangle|^2$ is equivalent to the Hönl-London Factor (HLF).

The Einstein coefficients $\mathrm{A}_{v'v''}$ for individual vibrational transitions $v'' \longrightarrow v'$, needed to determine the electronic and vibrational contribution to the dipole moment μ, are known [44]

$$\mu_{\mathrm{vib}}(v'; v'') = \mu_{\mathrm{el}}\sqrt{FCF_{v'v''}} = \sqrt{\frac{\mathrm{A}_{v'v''} 3h\varepsilon_0\lambda^3}{16\pi^3}}. \tag{A.2}$$

The algorithm to calculate the HLF for a mixed coupling scheme is given in [45]. It relies on the ratio γ of spin–orbit coupling coefficient A to the rotational constant B. With A and B from [46] using the fact that B is only weakly dependent on v'', we use here an average value of $\gamma = 74.5$.

The renormalized Hönl-London factors for the $^2\Sigma^+ \longrightarrow ^2\Pi_{1/2}$ transitions with $j'' = 1/2$ and $j'' = 3/2$ are given explicitly in Table 1. Using the Einstein coefficients from [44]

$$A_{0,0} = 1.002 \times 10^6\,\mathrm{s}^{-1} \longrightarrow \mu_{0,0} = 6.406 \times 10^{-31}\ \mathrm{Asm}$$
$$A_{0,6} = 8.801 \times 10^4\,\mathrm{s}^{-1} \longrightarrow \mu_{0,6} = 2.904 \times 10^{-31}\ \mathrm{Asm}$$

and linear polarized light ($\Delta m = 0$), the dipole matrix elements of the NO $\gamma(0,0)$ and $\gamma(0,6)$ bands were calculated and are also given in Table 1.

Table 2. Rabi frequencies of the pump- and Stokes transitions for several pulse energies W with $R = 1.5$ mm beam radius and pulse duration $\Delta\tau = 3$ ns. Ω_{P} and Ω_{S} are scaling with $\Omega^0\ \sqrt{W[\mu\mathrm{J}]}$ where $\Omega_{\mathrm{P}}^0 = 2\pi$ 54.2 MHz and $\Omega_{\mathrm{S}}^0 = 2\pi$ 24.7 MHz.

$W[\mu\mathrm{J}]$	$\Omega_{\mathrm{P}}/2\pi$ [MHz]	$\Omega_{\mathrm{S}}/2\pi$ [MHz]
1	54.2	24.7
5	121	55
10	172	78
50	383	174
100	542	247

A.2 Laser fieldstrengths

Assuming laser pulses of gaussian envelope $E(t) = E_0 \exp(-(t/\Delta\tau)^2)$, an homogeneous intensity distribution within a circular area of radius R and a pulse energy W, the electric field amplitude E_0 at the center of the pulse is given by

$$E_0 = \sqrt{\frac{W\ 2\sqrt{2}}{\pi^{3/2}R^2 c\varepsilon_0\Delta\tau}}. \tag{A.3}$$

Typical Rabi frequencies for the pump– and Stokes transitions ($j'' = 1/2$) ($^2\Pi_{1/2}(v'' = 0) \longrightarrow^2 \Sigma^+(v' = 0)$ with $\mu = 2.135{\times}10^{-31}$ Asm, and $^2\Sigma^+(v'{=}0) \longrightarrow ^2\Pi_{1/2}(v''{=}\ 6)$ with $\mu = 0.968 \times 10^{-31}$ Asm, respectively) are given in Table 2. The Stokes pulse energy needs to be a factor of five larger than the corresponding pump pulse energy to equalize both Rabi frequencies.

Appendix B: Relative transition strengths

For a full treatment the consequences of hyperfine splitting need to be considered. We determine the dipole moments for transitions between levels in the X–state with quantum

$$H_6 = -\frac{\hbar}{2}\begin{pmatrix} -2\Delta_P + \Delta_A & 0 & \frac{1}{3}\Omega_P & \sqrt{8/9}\Omega_P & 0 & 0 \\ 0 & -2\Delta_P - \Delta_A & \sqrt{8/9}\Omega_P & \frac{1}{3}\Omega_P & 0 & 0 \\ \frac{1}{3}\Omega_P & \sqrt{8/9}\Omega_P & \Delta_B & 0 & \frac{1}{3}\Omega_S & \sqrt{8/9}\Omega_S \\ \sqrt{8/9}\Omega_P & \frac{1}{3}\Omega_P & 0 & -\Delta_B & \sqrt{8/9}\Omega_S & \frac{1}{3}\Omega_S \\ 0 & 0 & \frac{1}{3}\Omega_S & \sqrt{8/9}\Omega_S & -2\Delta_S + \Delta_C & 0 \\ 0 & 0 & \sqrt{8/9}\Omega_S & \frac{1}{3}\Omega_S & 0 & -2\Delta_S - \Delta_C \end{pmatrix} \quad \text{(B.4)}$$

Table 3. Relative transition strengths S_q in units of $|\langle j', k'|d|j'',\ \Omega\rangle|^2$ for linear polarization $q = 0$ (see Eq. (B.1 and B.2)) with $j'' = j' = 1/2$ and $I = 1$.

	X	F"=3/2				F"=1/2	
A	M_F	3/2	1/2	-1/2	-3/2	1/2	-1/2
	3/2	9/54	-	-	-	-	-
F'=	1/2	-	1/54	-	-	8/54	-
3/2	-1/2	-	-	1/54	-	-	8/54
	-3/2	-	-	-	9/54	-	-
F'=	1/2	-	8/54	-	-	1/54	-
1/2	-1/2	-	-	8/54	-	-	1/54

numbers (v'', Ω, I, j'', F'', M_F'') and the A–state with quantum numbers (v', k', I, j', F', M_F'). The electronic and vibrational contributions may be separated according to ([22], Chap. 21)

$$\begin{aligned}\mu_{dip} &= \mu_{el}\sqrt{FCF(v', v'')} \\ &\quad \times\langle k', I, j', F', M_F'|d_q|\Omega, I, j'', F'', M_F''\rangle \\ &= \mu_{el}\sqrt{FCF(v', v'')\ HLF(j', k', j'', \Omega)} \\ &\quad \times(-1)^{j''+I+2F'-M_F'+1} \times \begin{pmatrix} F' & 1 & F'' \\ -M_F' & \Delta M & M_F'' \end{pmatrix} \\ &\quad \times\sqrt{(2F''+1)(2F'+1)} \times \begin{Bmatrix} j' & 1 & F' \\ F'' & I & j'' \end{Bmatrix}.\end{aligned} \quad \text{(B.1)}$$

The ratios of the relative transition strength factors

$$S_q = |\langle k', I, j', F', M_F'|d_q|\Omega, I, j'', F'', M_F''\rangle|^2 \quad \text{(B.2)}$$

to the Hönl-London factors $HLF(j', k', j'', \Omega)$, calculated from equation (B.1), are given in Table 3. With these relations the Hamiltonians in equations (2.1 and 2.2) read explicitly

$$H_3 = -\frac{\hbar}{2}\begin{pmatrix} -2\Delta_P - \Delta_A & \Omega_P & 0 \\ \Omega_P & -\Delta_B & \Omega_S \\ 0 & \Omega_S & -2\Delta_S - \Delta_C \end{pmatrix} \quad \text{(B.3)}$$

and see equation (B.4) *above*

where the coupling strength is given with reference to the Rabi frequencies in the three–state system, $\Omega_{12} = \Omega_P$ and $\Omega_{32} = \Omega_S$.

Appendix C: Coherent population return

The dynamics of the interaction of coherent radiation with a two level system is well known [22]. Here, we explain why a strong pulse of coherent radiation with smooth envelope does not lead to substantial saturation broadening. The understanding of this phenomenon is important for the normalization procedure of the transfer efficiency in a three level system.

Pulsed laser excitation with large pulse area and an interaction time much shorter than the lifetime of the excited state leads to Rabi oscillations. Figure 15 shows the population of the upper state after the interaction with a gaussian pulse or a pulse with a rectangular shape, both of them having the pulse area $\int\Omega(t)\mathrm{d}t = \sqrt{\pi}\Omega_{12}\Delta\tau$. The half width at 1/e with respect to the maximum of the former is $\Delta\tau$, while the duration of the latter is $\sqrt{\pi}\Delta\tau$. For on resonance tuning ($\Delta = 0$), the variation of the excitation probability is the same for both pulses. However, for $\Delta \neq 0$ the excitation dynamics is dramatically different. While substantial saturation broadening is observed for excitation with a pulse of rectangular shape, such broadening is not observed for a gaussian pulse.

The eigenstates of the Hamiltonian of the system

$$\hat{H}' = -\frac{\hbar}{2}\begin{pmatrix} -\Delta & \Omega(t) \\ \Omega^*(t) & \Delta \end{pmatrix} \quad \text{(C.1)}$$

are written in the basis of the bare states $|1\rangle$ and $|2\rangle$

$$|a^+\rangle = \cos\Theta|1\rangle - \sin\Theta|2\rangle \qquad |a^-\rangle = \sin\Theta|1\rangle + \cos\Theta|2\rangle \quad \text{(C.2)}$$

where

$$\tan\Theta = \frac{\Omega}{\sqrt{\Omega^2+\Delta^2}+\Delta} = \frac{\sqrt{\Omega^2+\Delta^2}-\Delta}{\Omega} \quad \text{(C.3)}$$

and the corresponding eigenvalues are

$$\omega^{\pm} = \pm\frac{1}{2}\sqrt{\Omega^2+\Delta^2}.$$

For $\Delta \neq 0$, we have $\tan\Theta = 0$ at very early and very late times ($\Omega(t) \ll |\Delta|$). Therefore $|\langle a^+|1\rangle| = 1$ at early and late times and no population remains in state $|2\rangle$ at the end of the pulse, provided the evolution is adiabatic, *i.e.* $|\dot{\Theta}| \ll |\omega^{\pm}|$. This phenomenon is known as "Complete Population Return" (CPR) [47]. For Gaussian pulses, the condition for adiabatic evolution is well satisfied and only little population is transferred from the initially populated state $|a^+\rangle$ to the state $|a^-\rangle$. Some of the population which reaches the latter will be in state $|2\rangle$ at the end of the interaction. For a Gaussian pulse excitation will only be observed for $\Delta < 1/\Delta\tau$.

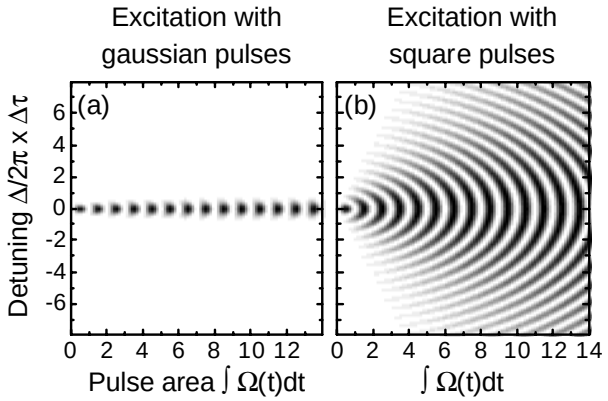

Fig. 15. Comparison of the excited state population in a two level system for gaussian pulses (a) and square pulses (b) of same pulse areas (square pulse duration $\sqrt{\pi}\Delta\tau$), as a function of the Rabi frequency Ω_{12} and laser detuning Δ_{12}.

The sudden increase of the Rabi frequency in case of the rectangular pulse leads to strong nonadiabatic coupling of the states $|a^+\rangle$ and $|a^-\rangle$ at the beginning and the end of the interaction. In the beginning the angle Θ increases suddenly to a value determined by the Rabi frequencies and the population in $|1\rangle$ is distributed accordingly to the dressed $|a^+\rangle$ and $|a^-\rangle$ states. At the end, the phase relation $\omega^+ t$ between the dressed states determines how the population projects back onto the bare states. Averaging over this relative phase, the final population in the upper state

$$\overline{|\langle 2|\Psi(t>0)\rangle|^2} = 2\sin^2\phi\ \cos^2\phi\ \overline{\sin^2(\omega^+ t)} \quad \text{(C.4)}$$
$$= \frac{\Omega^2}{2(\Omega^2+\Delta^2)},$$

shows the expected Lorentzian line profile with full width at half maximum $\Delta_{\mathrm{FWHM}} = \Omega$.

Appendix D: Dependence on the pulse shape

The envelope $E(t)$ of laser pulses often derivates from a gaussian shape. Here we examine the detrimental effect of asymmetry of the pulse shape. Such an asymmetry could be caused by a slow decay of the inversion in the Nd:YAG rod or nonlinear effects in the pulse amplifiers or the doubling crystals. Also Nd:YAG lasers with an internal phase conjugate mirror exhibit an intrinsic asymmetric pulse with a fast rise time and a slow decay.

For the purpose of demonstration, we assume the asymmetric pulse shape shown in Figure 16. The tails prevent the increase of the mixing angle to $\Theta = 90°$ as needed for complete transfer. Figure 16 shows the simulated time evolution of the population due to such pulses. Although at $t \approx 3$ ns, the population is transferred almost completely to the final level, a large fraction of it returns to the initial state. Furthermore, we note that the small

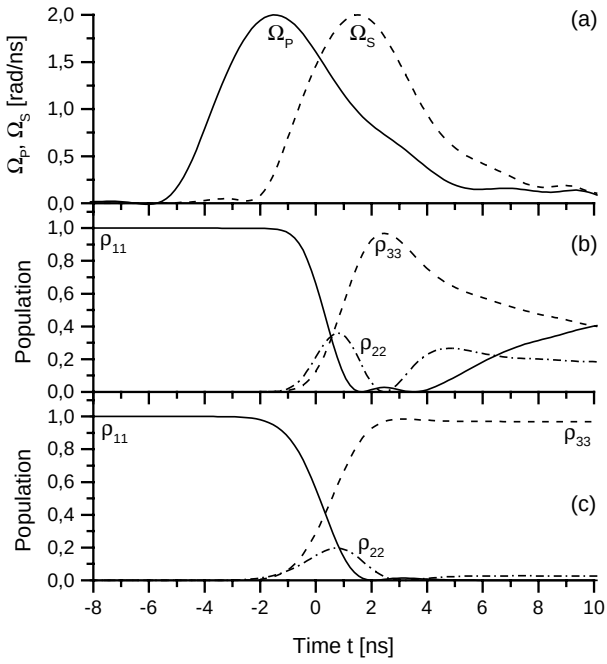

Fig. 16. Comparison of the population evolution (b) during the STIRAP excitation using a pulse envelope with tails (a) to the evolution using gaussian shaped pulses (c). The maxima of the Rabi frequencies $\Omega^0_{S,P} = 2\pi$ 320 MHz were chosen to fit the measured two photon linewidths.

Rabi frequencies in the tail do not assure adiabatic following and some population is lost by non-adiabatic coupling.

It is interesting to note that the determination of a pulse shape for most efficient transfer by the optimal control theory [48] leads to asymmetric forms. However, the optimal shape of the Stokes laser shows a slower rise and a faster fall, while the optimal shape of the pump laser is one with a faster rise and a slower fall.

References

1. K. Bergmann, B.W. Shore, in *Molecular Dynamics and Spectroscopy by Stimulated Emission Pumping*, edited by H.L. Dai and R.W. Field (World Scientific, Singapore, 1995) pp. 315–373.
2. J.R. Kuklinski, U. Gaubatz, F.T. Hioe, K. Bergmann, Phys. Rev. **A 40**, 6741–6744 (1989); U. Gaubatz, P. Rudecki, S. Schiemann, K. Bergmann, J. Chem. Phys. **92**, 5363–5376 (1990).
3. A. Kuhn, G.W. Coulston, G.Z. He, S. Schiemann, K. Bergmann, W.S. Warren, J. Chem. Phys. **96**, 4215–4223 (1992).
4. S. Schiemann, A. Kuhn, S. Steuerwald, K. Bergmann, Phys. Rev. Lett. **71**, 3637–3640 (1993).
5. T. Halfmann, K.Bergmann, J. Chem. Phys. **104**, 7068–7072 (1996).
6. P. Marte, P. Zoller, J.L. Hall, Phys. Rev. **A 44**, R4118–4121 (1991).
7. L.S. Goldner, C. Gerz, R.J. Spreeuw, S.L. Rollston, C.I. Westbrook, W.D. Phillips, P. Marte, P. Zoller, Phys. Rev. Lett. **72**, 997–1000 (1994).

8. J. Lawall, M. Prentiss, Phys. Rev. Lett. **72**, 993–996 (1994).
9. M. Weitz, B.C. Young, S. Chu, Phys. Rev. Lett. **73**, 2563–2566 (1994).
10. P.D. Featonby, G.S. Summy, J.L. Martin, H. Wu, K.P. Zerie, C.J. Foot, K. Burnett, Phys. Rev. **A 53**, 373 (1996).
11. J. Lawall, F. Bardou, B. Saubamea, K. Shimizu, M. Leduc, A. Aspect, C. Cohen–Tannoudji, Phys. Rev. Lett. **73**, 1915–1918 (1994);
    J. Lawall, S. Kulin, B. Saubamea, N. Bigelow, M. Leduc, C. Cohen–Tannoudji, *Proceeding of the 4th Intl. Workshop on Laser Physics* (Moscow, August 1995); Laser Physics **6**, 153–158 (1996).
12. T. Esslinger, F. Sander, M. Weidemüller, A. Hemmerich, T.W. Hänsch, Phys. Rev. Lett. **76**, 2432 (1996).
13. A. Kuhn, H. Perrin, W. Hänsel, C. Salomon, OSA TOPS on Ultracold Atoms and BEC, Vol.7, edited by K. Burnett, 58–65 (1996); S. Kulin, B. Saubamea, E. Peik, J. Lawall, T.W. Hijmans, M. Leduc, C. Cohen–Tannoudji, Phys. Rev. Lett. **78**, 4185 (1997).
14. R. Walser, J.I. Cirac, P. Zoller, Phys. Rev. Lett. **77**, 2658 (1996).
15. P. Dittmann, F.P. Pesl, J. Martin, G.W. Coulston, G.Z. He, K. Bergmann, J. Chem. Phys. **97**, 9472–9475 (1992).
16. M. Külz, M. Keil, A. Kortyna, B. Schellhaaß, J. Hauck, K. Bergmann, D. Weyh, W. Meyer, Phys. Rev. **A 53**, 3324–3334 (1996).
17. R. Sussmann, R. Neuhauser, H.J. Neusser, J. Chem. Phys **100**, 4784–4789 (1994); R. Sussmann, R. Neuhauser, H.J. Neusser, J. Chem. Phys. **103**, 3315 (1995); R. Neuhauser, R. Sussmann, H.J. Neusser, Phys. Rev. Lett. **74**, 3141–3144 (1995).
18. J. Oreg, F.T. Hioe, J.H. Eberly, Phys. Rev. A **29**, 690–697 (1984).
19. M.P. Fewell, B.W. Shore, K. Bergmann, Austr. J. Phys. **50**, 281–308 (1997).
20. G. Alzetta, A. Gozzini, L. Moi, G. Orriols, Nouvo Cimento **B36**, 5 (1976); E. Arimondo, G. Orriols, Lett. Nouv. Cim. **17**, 333 (1976).
21. S. Stenholm, *Foundations of Laser Spectroscopy* (J. Wiley&Sons, NY 1984).
22. B.W. Shore, *The theory of coherent atomic excitation* (J. Wiley& Sons, NY 1990).
23. G.W. Coulston, K. Bergmann, J. Chem. Phys. **96**, 3467–3475 (1992).
24. A. Vardi, M. Shapiro, J. Chem. Phys. **104**, 5490–5496 (1996).
25. B.W. Shore, J. Martin, M. Fewell, K. Bergmann, Phys. Rev. **A 52**, 566–582 (1995).
26. J. Martin, B.W. Shore, K. Bergmann, Phys. Rev. **A 52**, 583–593 (1995).
27. J. Martin, B.W. Shore, K. Bergmann, Phys. Rev. **A 54**, 1556–1569 (1996).
28. C.E. Carroll, F.T. Hioe, J. Phys. **A19**, 2061–2073 (1986); B.W. Shore, K. Bergmann, J. Oreg, Z. Phys. **D 23**, 33–39 (1992); M.V. Danileiko, V.I. Romanenko, L.P.Yatsenko, Opt. Comm. **109**, 462–466 (1994).
29. E. Hill, J.H. van Vleck, Phys. Rev. **32**, 250–272 (1928).
30. R.S. Mulliken, Rev. Mod. Phys. **3**, 89–115 (1931).
31. R. de Vivie, S.D. Peyerimhoff, J. Chem. Phys. **90**, 3660–3670 (1989).
32. X. Yang, E.H. Kim, A.M. Wodtke, J. Chem. Phys. **96**, 5111 (1992).
33. F.A. Blum, K.W. Nill, A.R. Calwa, T.C. Harman, Chem. Phys. Lett. **15**, 144–146 (1972); D. Feller, E.D. Glendening, E.A. McCullough Jr., R.J. Miller, J. Chem. Phys. **99**, 2829–2839 (1993).
34. T. Bergeman, R.N. Zare, J. Chem. Phys. **61**, 4500–4514 (1974); R.J. Miller, W.L. Glab, B.A. Bushaw, J. Chem. Phys. **91**, 3277–3279 (1989).
35. U. Fano, Phys. Rev. **124**, 1866–1878 (1961).
36. S.E. Harris, J.E. Field, A. Imamoğlu, Phys. Rev. Lett. **64**, 1107–1110 (1990); S.E. Harris, Phys. Rev. Lett. **70**, 552–555 (1993); S.E. Harris, Phys. Rev. Lett. **72**, 52–55 (1994); S.E. Harris, J.J. Macklin, Phys. Rev. **A 40**, 4135–4137.
37. J.H. Eberly, M.L. Pons, H.R. Haq, Phys. Rev. Lett. **72**, 56–59 (1994).
38. M. Fleischhauer, Phys. Rev. Lett. **72**, 989–992 (1994).
39. F.T. Hioe, R. Grobe, Phys. Rev. Lett. **73**, 2559–2562 (1994); R. Grobe, F.T. Hioe, J.H. Eberly, Phys. Rev. Lett. **73**, 3183–3186 (1994); A. Kasapi, M. Jain, G.Y. Yin, S.E. Harris, Phys. Rev. Lett. **74**, 2447–2450 (1995).
40. K.J. Boller, A. Imamoğlu, S.E. Harris, Phys. Rev. Lett. **66**, 2593–2596 (1991); J.E. Field, K.H. Hahn, S.E. Harris, Phys. Rev. Lett. **67**, 3062–3065 (1991).
41. Yong-qing Li, Shao-zheng Jin, Min Xiao, Phys. Rev. **A 51**, R1754–1757 (1995).
42. K. Bergmann, H. Theuer, B.W. Shore, Rev. Mod. Phys. (submitted).
43. C. Cohen–Tannoudji, B. Diu, F. Laloë, *Quantum mechanics*, Vol. 2, Chap. 10 (Hermann, Paris and J.Wiley&Sons, NY 1977).
44. L.G. Piper, L.M. Cowles, J. Chem. Phys. **85**, 2419–2422 (1986).
45. L.T. Earls, Phys. Rev. **48**, 423–424 (1935).
46. R. Engleman Jr., P.E. Rouse, J. Molec. Spectr. **37**, 240 (1971); R. Engleman Jr., P.E. Rouse, H.M. Peek, V.D. Baiamonte, Los Alamos Scientific Lab. Report LA–4364 UC–34 physics TID–4500, July 1970.
47. N.V. Vitanov, J. Phys. B **28**, L19–L22 (1995); N.V. Vitanov, P.L. Knight, J. Phys. B **28**, 1905–1920 (1995).
48. V. Malinovsky, D. Tannor, Phys. Rev. A (in press).